Modified foreign body reaction to silicone imbedded in subcutaneous tissues by different mouse systemic immune conditions

Tomohiro Yamakawa[1], Osamu Ichii[1,2*], Teppei Nakamura[1,3], Takashi Namba[1], Yaser Hosny Ali Elewa[1,4], Md. Abdul Masum[5], Yuki Otani[1], Takanori Nishimura[2,6], and Yasuhiro Kon[1]

[1]Laboratory of Anatomy, Department of Basic Veterinary Sciences, Faculty of Veterinary Medicine, Hokkaido University, Sapporo, Japan
[2]Laboratory of Agrobiomedical Science, Faculty of Agriculture, Hokkaido University, Sapporo, Japan
[3]Department of Biological Safety Research, Chitose Laboratory, Japan Food Research Laboratories, Chitose, Japan
[4]Department of Histology, Faculty of Veterinary Medicine, Zagazig University, Zagazig, Egypt
[5]Department of Anatomy, Histology and Physiology, Faculty of Animal Science and Veterinary Medicine, Sher-e-Bangla Agricultural University, Dhaka, Bangladesh
[6]Laboratory of Cell and Tissue Biology, Research Faculty of Agriculture, Hokkaido University, Sapporo, Japan.

*Corresponding author: Osamu Ichii, DVM, PhD
Laboratory of Anatomy, Department of Basic Veterinary Sciences, Faculty of Veterinary Medicine, Hokkaido University, Kita 18, Nishi 9, Kita-ku, Sapporo 060-0818, Japan
E-mail: ichi-o@vetmed.hokudai.ac.jp
Tel./Fax: +81-11-706-5188

Running title: Immunity and foreign body reaction

Acknowledgments: NA

Funding: NA

Conflict of interest: The authors have no conflicts of interest directly relevant to the content of this article.

Ethics approval: All animal experiments were approved by the Institutional Animal Care and Use Committee of Hokkaido University and the Faculty of Veterinary Medicine, Hokkaido University (approval No. 17-0133, 21-0008). Our animal experiments program was approved by the Association

for Assessment and Accreditation of Laboratory Animal Care International.

ABSTRACT

Foreign body reaction (FBR) causes unexpected adverse effects due to implanted materials in humans and animals. Inflammation and subsequent fibrosis during FBR seems to be affected by recipient immunity, such as the balance of T helper (Th) response, that has the potential to regulate FBR-related macrophage function. Here, the immunological effects of FBR on subcutaneously imbedded silicone tubes (ST) at 8 weeks were investigated histologically by comparing Th1-biased C57BL/6N, Th2-biased MRL/MpJ, and autoimmune disease-prone MRL/MpJ-*Fas*$^{lpr/lpr}$. Tissue surrounding ST (TSS) was analyzed at day (D) 7 and 14 (reaction phase) or D35 (stability phase) after surgery. In all strains, the TSS was composed of a thin layer (TL) containing fibrous tissues and loose connective tissues formed outside the TL. Few lymphocytes and mast cells, several neutrophils, and numerous macrophages infiltrated the TSS. Active vascularization was observed at D14 in all strains. For the examined indices, M1-type macrophage density in the TSS of C57BL/6N mice was significantly higher at D14 compared to other strains. No significant strain difference relating to M2-type macrophages was detected, suggesting the effects of Th1-biased immunity on FBR-related inflammation. Collagen fibers in the TSS increased in density and became stable with age in all strains. In particular, MRL/MpJ-*Fas*$^{lpr/lpr}$ showed progressive fibrotic features. Serum autoantibody levels in MRL/MpJ-*Fas*$^{lpr/lpr}$ mice were inversely correlated with M1-type macrophage density. These data from MRL/MpJ-*Fas*$^{lpr/lpr}$ mice suggested modifications of FBR-related inflammation and fibrosis by autoimmune abnormalities. The results provide crucial insights into the pathological modification of FBR by recipient immunity and emphasize its clinicopathological importance in humans and animals.
Keywords: foreign body reaction, silicone, inflammation, fibrosis, macrophage

INTRODUCTION

Foreign body reaction (FBR) to implanted materials can cause unexpected adverse effects. In general, the biological processes during FBR consist of two main reactions: inflammation and subsequent fibrosis. In particular, in human medicine, FBR is observed around transplanted grafts or implanted medical devices. Infection, excessive inflammation, or fibrosis follows the local pathogenic FBR *in situ* (1). Fibrotic tissue produced by FBR can affect the function of intravenously implanted glucose sensors in humans (2). During FBR, immune cells, especially macrophages, play crucial roles in both inflammation and fibrosis (1). In a previous study, FBRs to silicone tubes (STs) subcutaneously embedded in the back skin of ICR mice were divided into two main stages (3). Briefly, the early stage of FBR mainly proceeded to an innate immune response characterized by infiltration of neutrophils and macrophages around the ST. The later stage developed and stabilized the connective tissue surrounding the ST (3). It is necessary to understand the clinicopathological significance of FBRs to

elucidate the spatiotemporal alteration of tissues surrounding the foreign body, especially focusing on inflammation and fibrosis.

Pathological features of local inflammation and subsequent fibrosis are strongly affected by the status of systemic immunity. For the former process, it has been reported that human patients with rheumatoid arthritis show a higher expression of vascular endothelial growth factor receptor at the site of inflammation at the time of wounding, indicating more active angiogenesis compared with healthy subjects (4). Importantly, relapses and flares with delayed wound healing are one of the representative symptoms in human clinical cases of systemic lupus erythematosus (SLE), an autoimmune disease (5). These phenotypes of human SLE patients are strongly affected by the functional alternation of T helper (Th) cells and macrophages (6, 7), suggesting the possibility of similar modification effects of this inflammatory disease on the tissue remodeling process. Furthermore, it has been reported that hypoxia-inducible factor 1 is highly expressed in human skin for autoimmune diseases, including systemic sclerosis, and acts as a stimulator of fibrosis (8). Thus, although the tissue remodeling process with local inflammation and fibrosis is affected by the systemic immune conditions of human patients or animal models, there has been scarce information relating their effects or modifications in the progression of FBR.

Importantly, the dynamics of macrophages depend on the systemic or local immune status of individuals. In particular, the *in vivo* balance of the Th response, one of the main factors altering the progression of immune reactions, influences the differentiation and activation of macrophages. Briefly, Th1 and Th2 responses are important for cellular and humoral immunity, respectively (9). In general, Th1 induces the differentiation of macrophages to the M1-type, which has inflammatory effects and plays a central role in cellular immunity (9). On the other hand, Th2 induces their differentiation into the M2-type, which is involved in anti-inflammation and tissue repair (9). Systemic Th1/Th2 balance is altered by various factors, such as disease and aging (10, 11), and Th1 predominance changes with age in dogs and cats (12).

Inbred C57BL/6N (B6) is a representative murine strain for healthy control, and it is known that several inbred strains, including B10D2 and B6, show a Th1-biased response (9). In contrast, Balb/c, DBA/2, and MRL/MpJ (MRL) show a Th2-biased response; in particular, MRL is an inbred strain that manifests as unique tissue repair phenotypes, such as healing ear and corneal wounds without scarring (13, 14). Furthermore, the mutant strain MRL/MpJ-*Fas*$^{lpr/lpr}$ (lpr), manifests as severe systemic autoimmune disease characterized by the production of anti-double stranded DNA (dsDNA) autoantibodies as well as the development of hyperinflammatory phenotypes, including glomerulonephritis, arthritis, and vasculitis (13, 14). These autoimmune phenotypes are caused by mutations in the apoptosis-related gene *Fas* that encodes tumor necrosis factor receptor superfamily

member 6 (13, 14). In a previous study, we revealed the spatiotemporal alteration of subcutaneous tissues surrounding imbedded STs in an outbred ICR strain (3). Based on these methods and findings, the present study analyzed the modification features and mechanisms of FBR due to the differences in immunological status by using the Th1-biased B6, Th2-biased MRL, and autoimmune disease-prone lpr mice.

Inflammatory features during FBR were more prominent in Th1-biased B6 mice than in MRL-type genomic background strains, while lpr mice with severe autoimmune diseases manifested more progressive fibrotic features. This study provides basic knowledge clarifying the effect of systemic immune status on FBR in human and veterinary medicine.

MATERIALS AND METHODS

Animals

Male B6, MRL, and lpr mice were purchased from Japan SLC, Inc. (Hamamatsu, Japan) and maintained under specific pathogen-free conditions. Animal experimentation was approved by the Institutional Animal Care and Use Committee of the Faculty of Veterinary Medicine, Hokkaido University (approval no. 17-0133, 21-0008). The animals were handled in accordance with the Guide for the Care and Use of Laboratory Animals, Faculty of Veterinary Medicine, Hokkaido University (approved by the Association for Assessment and Accreditation of Laboratory Animal Care International).

Surgical imbedding of silicon tube

Surgeries were performed according to a previous study (3). At 8 weeks of age, mice were anesthetized by intraperitoneal injection of a mixture of medetomidine (0.3 mg/kg), midazolam (4 mg/kg), and butorphanol (5 mg/kg). The dorsal skin was shaved, disinfected, and incised approximately 5 mm long according to the left-right axis of mice. Sterilized ST (1 mm × 20 mm) was embedded in the subcutaneous pouch and the wound was closed antiseptically using absorbable suture (M684R; Matsudaika Kogyo Co., Ltd., Tokyo, Japan). Recovery of the mice was aided by the intraperitoneal (i.p.) injection of atipamezole (0.3 mg/kg) under a warm condition and i.p. administration of ampicillin (1 mg/kg). At day (D) 7, 14, and 35 following surgery, mice were euthanized by blood vessel cannulation in the femoral artery and cervical dislocation under deep anesthesia using a mixture of medetomidine, midazolam, and butorphanol. The skin with ST was collected. The ST was easily retrieved because it was weakly attached to the subcutaneous tissues, as described previously (3). D7 and D14 were considered as the reaction phases in the previous study (3). D35 was selected as the stability phase.

Evaluation of systemic immune condition

The ratio of spleen weight (SPW) to body weight (BW) was calculated. Serum levels of anti- dsDNA antibody were measured to evaluate systemic immune conditions using the LBIS Anti-dsDNA-Mouse ELISA Kit (FUJIFILM Wako Pure Chemical Corporation, Osaka, Japan) according to the manufacturer's instructions.

Histological analysis

Collected samples were fixed with 4% paraformaldehyde at 4°C overnight, embedded in paraffin, and cut into sections (3 or 4 μm thick). The sections including the cross section of imbedded ST from

the rostral direction. Deparaffinized sections were stained with hematoxylin-eosin (HE), Masson's trichrome (MT), or toluidine blue (TB) and analyzed by immunohistochemistry (IHC) or immunofluorescence (IF).

Immunohistochemistry and Immunofluorescence

Immunohistochemistry for CD3, B220, Gr-1, CD31, CD68, and CD204 was performed to detect T cells, B cells, granulocytes, vascular endothelial cells, M1-type macrophages, and M2-type macrophages as previously described (3). The paraffin sections were deparaffinized, and antigen retrieval was performed. Subsequently, to block internal peroxidase activity, the sections were soaked in methanol containing 0.3% H_2O_2 for 20 min at 25°C. After washing three times in phosphate-buffered saline (PBS), the sections were incubated with blocking serum for 1 h at 25°C to block non-specific reactions. The sections were then incubated with primary antibodies overnight at 4°C. The sections were then washed three times in PBS, incubated with secondary antibodies for 30 min at 25°C, and washed three times in PBS. The sections were then incubated with streptavidin-conjugated horseradish peroxidase using a SABPO® kit (Nichirei, Tokyo, Japan) for 30 min at 25°C and washed three times in PBS. The immunopositive reaction was visualized using 3,3' -diaminobenzidine tetrahydrochloride in 0.05 M Tris-H_2O_2 solution. Finally, sections were stained with hematoxylin. Details of the antibody, antigen retrieval, and blocking are listed in Table 1.

Immunofluorescence was performed to detect CD68- or CD204-positive cells. The paraffin sections were deparaffinized, antigen retrieved, and blocked using normal serum for IHC. After overnight incubation with the primary antibody at 4°C, the sections were incubated with secondary antibody for 1 h at 25°C. The sections were observed by fluorescence microscopy using a model BZX-710 microscope (Keyence, Osaka, Japan). The details of antigen retrieval, dilution, and antibodies are listed in Table 1.

Histoplanimetry

Inflammatory indices in tissue surrounding the ST

A TL was formed at the border between the ST and subcutaneous tissues (3). Images of TSS, including both TL and loose connective tissue (LCT) around the ST, were obtained at 40× magnification in sections stained with HE. The total area of tissue surrounding the ST (TSS) and the total number of cell nuclei in this area were quantified using a BX-analyzer (Keyence). The cell density (number/mm^2) represented the total cell number. Similarly, the cell densities of CD31, Gr-1, CD68, and CD204 IHC-positive cells were also evaluated. Ten or more images were used for histoplanimetry.

Fibrous alternation indices in TSS

MT-stained sections were converted to virtual slides using Nano Zoomer 2.0 RS (Hamamatsu Photonics Co., Ltd., Hamamatsu, Japan). Measurements were performed using an NDP view2 (Hamamatsu Photonics Co., Ltd.). To measure TL thickness, a straight line parallel and perpendicular to the skin was drawn from the center of the ST. The thickness was measured at the intersection of these straight lines and the TL represented the total of four areas (Supplemental figure 1). This measurement was performed on one section of each sample.

Ten or more images of TSS were obtained at 40× magnification in MT sections. The aniline blue-positive portion of the measured area (%) was quantified using a BX-analyzer (Keyence) and expressed as the density of collagen fibers.

Statistical analyses

Results are expressed as the mean ± standard error (SE) and analyzed using non-parametric statistical methods. The Kruskal–Wallis test was used to compare the numerical results, and multiple comparisons were performed using Scheffe's method when significant differences were observed (P<0.05). The correlation coefficients of the various indices were evaluated using Spearman's rank coefficient (P<0.05).

RESULTS

Systemic immune condition

The SPW/BW ratio and serum anti-dsDNA antibody levels were evaluated as indicators of systemic immunity (Fig. 1). B6 and lpr mice displayed significantly higher SPW/BW ratio compared with MRL, with no changes with time. Since B6 mice weighed approximately half compared to that of MRL and lpr mice, SPW/BW was relatively high. MRL and lpr mice had similar BW, but the SPW of lpr mice was approximately twice compared to that of MRL mice, indicating the presence of autoimmune abnormalities in lpr mice. Serum anti-dsDNA antibody, a representative index of autoimmune disease, was the highest in lpr mice, with a significant difference compared to other strains, with no changes over time.

Morphological changes of TSS

Fig. 2 shows the HE-stained cross sections of TSS with skin and summarizes the histological alteration of TSS. In all strains and examined days, circular TSS. The ST usually detached from the slide glasses during sectioning or staining (Fig. 2A).

In all strains and examined days, TSS was composed of TL and LCT (Fig. 2B–D). TL formed adjacent to the ST and LCT formed just outside of the TL. Their borders were clearly identified on HE-stained sections. TLs were composed of dense fibrous tissue and infiltrating mononuclear cells (Fig. 2B–D). In contrast, LCT was composed of scattered mononuclear cells and loose fibrous tissue. In B6 mice, cell infiltration increased from D7 to D14, but was decreased at D35 (Fig. 2B). Notably, numerous infiltrating cells were observed in the TL at D14 of B6 mice (Fig. 2B). In contrast, the cell infiltrations in TSS samples of MRL and lpr mice were relatively mild compared to B6 mice (Fig. 2C and D).

For histoplanimetry, the total cell number in the TSS of B6 mice was highest at D14, and was significantly different at D14 compared to the value for MRL and lpr mice. (Fig. 2E). Although no significant time-related alternations were observed in the total cell number in the TSS of MRL mice, that of lpr mice at D35 was significantly lower compared to other examined days and B6 and MRL on the same day (Fig. 2E).

Inflammatory cells in TSS

Figure 3 shows IHC- or TB-stained representative sections of TSS with skin at D14. Several $CD3^+$ T cells, $B220^+$ B cells, and metachromatic mast cells were observed in the mouse LCTs without remarkable strain- or time-related differences during the observation period (Fig. 3A–C). These mild infiltrations of these cells indicated that an excessive FBR, as observed in rejection response to

biomaterials (15), did not occur.

On the other hand, infiltrating Gr-1$^+$ neutrophils were more commonly observed in both TL and LCT than in lymphocytes and mast cells, and they appeared at D7 (Fig. 4A). To evaluate angiogenesis, a major event during inflammation, we examined CD31$^+$ vascular endothelial cells on IHC sections. CD31$^+$ vessels were mainly observed in the LCT and appeared to be abundant at D14 in all strains (Fig. 4B).

Figure 4C shows the results of histoplanimetry for Gr-1$^+$ neutrophils and CD31$^+$ vessels. The density of Gr-1$^+$ neutrophils showed a decreasing tendency from D7 to D35 in all strains without time- or strain-related differences (Fig. 4C). Furthermore, the density of CD31$^+$ vessels was highest at D14 in all strains, and a significant difference between D7 and D14 was detected in B6 (Fig. 4D). In all strains, the density of CD31$^+$ cells significantly decreased from D14 to D35 (Fig. 4D).

Macrophages are crucial inflammatory cells in FBRs (1). In general, M1- and M2-type macrophages differentiate from inflammatory monocytes and resident macrophages involved in tissue repair, respectively (16). Figure 5A shows the findings for TSS examined by IF for CD68 and CD204 in B6 at D14 and cell markers for M1- and M2-type macrophages. Briefly, CD68$^+$ or CD204$^+$ macrophages tended to localize to the TL or LCT, respectively.

Similarly, for IHC, CD68$^+$ macrophages were mainly observed in the TL of all strains (Fig. 5B–D). Characteristically, B6 mice at D14 showed numerous CD68$^+$ macrophages in the TL. They showed various morphologies, such as abundant cytoplasm or multi-nucleic features (Fig. 5B). On the other hand, CD68$^+$ macrophages of B6 mice at D35 and other strains at all examined periods showed a narrow cytoplasm or squamous shape in TL (Fig. 5B–D).

For histoplanimetry, the number of CD68$^+$ macrophages in B6 mice significantly increased from D7 to D14, and that at D14 was significantly higher than that of the other strains (Fig. 5E). Furthermore, B6 mice displayed a significant decrease from D14 to D35 (Fig. 5E). In MRL mice, the number of CD68$^+$ macrophages was the highest at D7 and significantly decreased from D7 to D14 and D35. Furthermore, the lpr at D35 was significantly lower than that at D7 and D14.

Similar to IF, scatter CD204$^+$ macrophages localized to LCT without remarkable strain- or time-course-related differences, and almost all positive cells showed oval or round shapes (Fig. 6A–C).

For histoplanimetry, the number of CD204$^+$ macrophages in all strains was the highest at D7 in all examination periods and tended to decrease over time, but there were no significant strain- or time course-related differences (Fig. 6D).

Fibrotic reaction in TSS

Figure 7A–C shows the MT-stained cross sections of TSS with skin that was performed to evaluate

the fibrotic reaction. In MT-stained sections, the tissue appeared to become more aniline blue-positive and darker in color over time. This seemed to be especially true for lpr mice (Fig. 7C).

For histoplanimetry, the TLs of B6 and lpr mice tended to be thickened from D7 to D14, and their values decreased from D14 to D35 without significance (Fig. 7D). On the other hand, MRL mice showed constant lower values compared with other strains over the examined time, and significant differences were observed with B6 mice at all examined points.

The density of collagen fibers tended to increase during the examined period, and lpr mice showed significantly higher values than B6 mice at D7. Significant differences between D7 and D35 were detected in lpr mice (Fig. 7E).

Correlation among histological parameters and immune-related indices

Table 2 shows the correlation between histological indices of TSS components and fibrosis using data from all strains. Briefly, TL thickness was significantly and positively correlated with total cell number and $CD68^+$ cell number in TSS. In contrast, the density of collagen fibers was significantly and negatively correlated with total cell number, $CD68^+$ cell number, and $CD204^+$ cell number.

Table 3 shows the correlation between histological indices of TSS and systemic immunity indices using the data from lpr mice. The SPW/BW ratio was not correlated with the examined parameters, but serum anti-dsDNA antibody levels showed a significant inverse correlation with $CD68^+$ cell number.

DISCUSSION

The present study examined B6, MRL, and lpr mouse models with Th1-biased, Th2-type biased, and autoimmune-prone phenotypes, respectively (17). The MRL mouse strain is a healthy control strain with the same genomic background as the lpr strain (18). As a result, all strains formed a subcutaneous TSS consisting of TL and LCT, as reported in the ICR strain (3). Although systemic immune status indicated by the SPW/BW ratio and autoantibody production differed among strains, their TSS showed similar inflammation and fibrosis, and the histological features of TSS were altered with time after embedding of ST. In general, TLs of all strains were thin and relatively dense. However, the LCT, outer layer of TL, was somewhat rough, as reported in a previous study using ICR strain (3). Therefore, it is likely that FBR to ST, a material with low biological reactivity (19), proceeds to form TSS composed of two layers regardless of the genomic- or immune-related backgrounds of mice. When the same experiment was conducted with both silicone and latex, there was a noticeable difference in the course of the experiment (20). Future studies are needed to verify the relationship between FBRs and other materials and their immunological status.

According to a previous study (3), the process of FBR to ST can be divided into two major phases: the reaction phase and stability phase. Based on the results of the previous study, we performed experiments with D7 and D14 as the reaction phase and D35 as the stability phase. In all strains, TL and LCT were formed from D7, followed by histological development and stabilization of TL and LCT, characterized by alignment of fibers in a constant direction and accumulation of either cellular or fiber components. As common features of TSS among strains in the reaction phase, Gr-1$^+$ neutrophils appeared from D7 and were decreased at D14, and CD31$^+$ vascular endothelial cells increased from D7 to D14. During this phase, neutrophils regulate many immune signals (9). These signals include those that suppress neutrophils themselves and those that activate monocytes and macrophages (3). In FBRs to biomaterials, such as biomedical polymers, angiogenesis is most active in the chronic phase after the acute phase of the inflammatory response (21). Although there are some differences among strains, it is evident that innate immune responses, mainly the activation of neutrophils and macrophages, occur in the reactive phase.

Furthermore, in the reaction phase, the dynamics of CD68$^+$ macrophages differed among strains. CD68$^+$ macrophages appeared from D7 in all strains, but only B6 mice showed a transient increase in CD68$^+$ macrophages at D14. A similar tendency was observed in the total cell number in B6 mice. Since these mice have a Th1-type biased immune balance, they are susceptible to signals that promote the differentiation of macrophages into the M1-type, known as inflammatory macrophages (16). In contrast, MRL and lpr mice did not show an increase in inflammatory indices at D14, but rather displayed a decrease. This difference in the immune background between B6 mice and the

other strains may have led to an increase in the number of cells positive for CD68, an M1 macrophage marker (17). In contrast, $CD204^+$ cells showed similar kinetics to neutrophils in that they were abundant at D7 and then decreased. In the present study, CD204 was used as a marker of M2-type macrophages. In general, M2-type macrophages are differentiated and activated after the inflammatory response and play a role in suppressing inflammation and promoting angiogenesis and tissue repair (22). The findings suggest that the anti-inflammatory effect of macrophages generally follows inflammation. The present study was limited in that the quantitative evaluation of M2-type macrophages in the TSS began at D7. Their dynamics before D7 should be clarified.

In the stability phase from D14 to D35, almost all indices for inflammation were unchanged or decreased, but the density of collagen fibers tended to increase with time in all strains. These data indicate that fibrosis progressed in all the strains. However, the phenotype of lpr mice differed from the other strains in terms of the fibrosis index. Compared with other strains, collagen fiber density was significantly higher at D7, indicating that autoimmune diseases may have some effect on the fibrosis process. It is possible that the inflammatory phase occurred earlier than B6 and was already in the stable phase by D7. There was an inverse correlation between serum anti-dsDNA antibody levels and the number of $CD68^+$ macrophages. It has been reported that autoimmune diseases are largely related to the differentiation and functional roles of macrophages (23, 24). In this study, there was no significant difference in the dynamics of M1-type macrophages between MRL and lpr mice. However, it is possible that the functional role of macrophages is affected by autoimmunity, leading to increased fibrosis in lpr mice.

CONCLUSION

In conclusion (Fig. 8), TSS is composed of TL and LCT, and the effect of immune status on tissue architecture was not significant in the long term, but resulted in significant differences in inflammatory responses and morphological changes in the short term. B6 with a Th1-type immune background has a higher expression of $CD68^+$ macrophages, which may have increased tissue formation and immune responses. On the other hand, the expression of $CD68^+$ macrophages was suppressed even in the reaction phase in MRLs with a Th2-type immune background, resulting in less cell-dynamic FBRs. Lpr mice showed a similar course of FBR to MRL, with a slightly earlier onset of fibrosis and more advanced fibrosis, but no exacerbation of FBR due to autoimmune disease. This study provides insights into the pathogenesis of FBR and the importance of systemic immunity in FBR in human and veterinary medicine.

REFERENCES

1. Anderson JM, Rodriguez A, Chang DT. Foreign body reaction to biomaterials. *Sem. Immunol.* 2008; *20(2)*: 86–100.
2. Ward WK, Wood MD, Troupe JE. Rise in Background Current over Time in a Subcutaneous Glucose Sensor in the Rabbit: Relevance to Calibration and Accuracy. *Biosens. Bioelectr.* 2000; *15*: 53–61.
3. Oe S, Masum MA, Ichii O, Nishimura T, Nakamura T, Namba T, Otani Y, Nakayama Y, Elewa YHA, Kon Y. Spatiotemporal histological changes observed in mouse subcutaneous tissues during the foreign body reaction to silicone*. J Biomed Mater Res A*. 2021; *109(7)*: 1220–1231.
4. Yoo SA, Yoon HJ, Kim HS, Chae CB, De Falco S, Cho CS, Kim WU. Objective Role of placenta growth factor and its receptor flt-1 in rheumatoid inflammation: A link between angiogenesis and inflammation. *Arthr. Rheum.* 2009; *60(2)*: 345–354.
5. Eghbalpour F, Aghaei M, Ebrahimi M, Tahsili MR, Golalipour M, Mohammad S, Yazdani Y. Effect of indole-3-carbinol on transcriptional profiling of wound-healing genes in macrophages of systemic lupus erythematosus patients: an RNA sequencing assay. *Lupus*. 2020; 29(8): 954–963.
6. Crayne CB, Albeituni S, Nichols KE, Cron RQ. The immunology of macrophage activation syndrome. *Front. Immunol.* 2019; *10*: 119.
7. Talaat RM, Mohamed SF, Bassyouni IH, Raouf AA. Th1/Th2/Th17/Treg cytokine imbalance in systemic lupus erythematosus (SLE) patients: Correlation with disease activity. *Cytokine*, 2015; *72(2)*: 146–153.
8. Deng W, Feng X, Li X, Wang D, Sun L. Hypoxia-inducible factor 1 in autoimmune diseases. *Cell. Immunol*. 2016; *303*: 7–15.
9. Mariani E, Lisignoli G, Borzì RM, Pulsatelli L. Biomaterials: Foreign bodies or tuners for the immune response? *Internat. J. Mol. Sci*. 2019; *20(3)*: 636.
10. Jing Y, Gravenstein S, Rao Chaganty N, Chen N, Lyerly KH, Joyce S, Deng Y. Aging is associated with a rapid decline in frequency, alterations in subset composition, and enhanced Th2 response in CD1d-restricted NKT cells from human peripheral blood. *Exp. Gerontol*. 2007; *42(8)*: 719–732.
11. Zhang C, Xiao C, Wang P, Xu W, Zhang A, Li Q, Xu X. The alteration of Th1/Th2/Th17/Treg paradigm in patients with type 2 diabetes mellitus: Relationship with diabetic nephropathy. *Hum. Immunol*. 2014; *75(4)*: 289–296.
12. Horiuchi Y, Nakajima Y, Nariai Y, Asanuma H, Kuwabara M, Yukawa M. Th1/Th2 balance in canine peripheral blood lymphocytes-A flow cytometric study. *Vet. Immunol. Immunopathol*. 2007; *118(3-4)*: 179–185.
13. Heydemann A. The super super-healing MRL mouse strain. *Front. Biol*. 2012; *7(6)*: 522–538.
14. Jabs DA, Lee B, Whittum-Hudson JA, Prendergast RA. Th1 Versus Th2 Immune Responses in

Autoimmune Lacrimal Gland Disease in MRL/Mp Mice. *Invest. Ophthalmol. Vis. Sci*. 2000; *41*: 826–831.

15. Jones KS. Effects of biomaterial-induced inflammation on fibrosis and rejection. *Sem. Immunol*. 2008; *20(2)*: 130–136.
16. Yunna C, Mengru H, Lei W, Weidong C. Macrophage M1/M2 polarization. *Eur. J. Pharmacol*. 2020; *877*: 173090
17. Orecchioni M, Ghosheh Y, Pramod AB, Ley K. Macrophage polarization: Different gene signatures in M1(Lps+) vs. Classically and M2(LPS-) vs. Alternatively activated macrophages. *Front. Immunol*. 2019; *10*: 1084.
18. Hosotani M, Ichii O, Nakamura T, Kanazawa SO, Elewa YHA, Kon Y. Autoimmune abnormality affects ovulation and oocyte-pick-up in MRL/MpJ-Fas lpr/lpr mice. *Lupus*. 2018; *27(1)*: 82–94.
19. Henstock JR, Canham LT, Anderson SI. Silicon: The evolution of its use in biomaterials. *Acta Biomaterialia*, 2015; *11(1)*: 17–26.
20. Koivusalo A, Mäikisalo H, Talja M, Cormio L, Ruutu M, Wolff H, Höckerstedt K. Experimental Medicine Biocompatibility of Latex and Silicone T Tubes in the Porcine Common Bile Duct: An Experimental Study. *Res. Exp. Med*. 1996; 196: 53–66.
21. Babensee JE, Anderson JM, Mcintire LV, Mikos AG. Host Response to Tissue Engineered Devices. *Adv. Drug Del. Rev*. 1998; 33: 111–139.
22. Mills CD, Kincaid K, Alt JM, Heilman MJ, Hill AM. M-1/M-2 Macrophages and the Th1/Th2 Paradigm. *J. Immunol*. 2000; *164(12)*: 6166–6173.
23. Funes SC, Rios M, Escobar-Vera J, Kalergis AM. Implications of macrophage polarization in autoimmunity. *Immunology*. 2018; *154(2)*: 186–195.
24. Tardito S, Martinelli G, Soldano S, Paolino S, Pacini G, Patane M, Alessandri E, Smith V, Cutolo M. Macrophage M1/M2 polarization and rheumatoid arthritis: A systematic review. *Autoimm. Rev*. 2019; *18(11)*: 102397.

FIGURE LEGENDS

Figure 1. Autoimmune disease indices

(A) Ratio of spleen weight (SPW) to body weight (BW).

(B) Serum levels of anti-dsDNA antibody.

B6: C57BL/6N. MRL: MRL/MpJ. lpr: MRL/MpJ-*Fas*$^{lpr/lpr}$. Each bar represents the mean ± SE (n ≥ 4). *: Significance with the other strain at same age (Kruskal-Wallis followed by Scheffe's method, $P<0.05$)

Figure 2. Histological characteristics of TSS

(A) Histology of TSS with skin at low magnification in D14.

(B–D) Histology of TSS at high magnification.

TSS: tissue surrounding silicone; TL: thin layer; ST: silicone tube; arrows indicate TL; HE staining. Bars = 500 μm in panel A and 200 μm in panels B–D.

(E) Total number of cells in TSS.

B6: C57BL/6N. MRL: MRL/MpJ. lpr: MRL/MpJ-*Fas*$^{lpr/lpr}$. Each bar represents the mean ± SE (n ≥ 4). Significance with the other age in B6 mice (*), lpr mice (#), B6 mice (B), MRL mice (M), and lpr mice (l) at the same age (Kruskal-Wallis followed by Scheffe's test, $P<0.05$).

Figure 3. Immune cells in TSS

(A) CD3 for T cells in TSS.

(B) B220 for B cells in TSS.

(C) TB staining for mast cells in TSS.

IHC images (panels A and B) and TB staining (panel C) at D14. Arrowheads indicate positive cells for IHC or metachromasy mast cells. Bars = 200 μm.

Figure 4. Neutrophils and vascular endothelial cells in TSS

(A) Gr-1 for neutrophils in TSS.

(B) CD31 for vascular endothelial cells in TSS.

Arrowheads indicate cells positive for IHC. Bars = 200 μm.

(C) Density of Gr-1$^+$ cells.

(D) Density of CD31$^+$ cells.

B6: C57BL/6N. MRL: MRL/MpJ. lpr: MRL/MpJ-*Fas*$^{lpr/lpr}$. Each bar represents the mean ± SE (n ≥ 4). Significance with the other age in B6 mice (*), MRL mice (†), and lpr mice (#) or with B6 mice (B), MRL mice (M), and lpr mice (l) at the same age (Kruskal-Wallis followed by Scheffe's test, $P<0.05$).

Figure 5. Macrophages in TSS

(A) CD68 (green) for M1-type and CD204 (red) for M2-type macrophage in the TSS of B6 at D14. IF, nuclear staining by Hoechst 33342.

(B–D) CD68 for M1-type macrophages in TSS. IHC.

Arrowheads indicate the positive cells for IHC. Bars = 200 μm.

(E) Density of $CD68^+$ cells.

B6: C57BL/6N. MRL: MRL/MpJ. lpr: MRL/MpJ-*Fas*$^{lpr/lpr}$. Each bar represents the mean ± SE (n ≥ 4). Significance with the other age in B6 mice (∗), MRL mice (†), and lpr mice (#) or with B6 mice (B), MRL mice (M), and lpr mice (l) at the same age (Kruskal-Wallis followed by Scheffe's test, $P<0.05$).

Figure 6. M2-type macrophage in TSS.

(A–C) CD204 for M2-type macrophages in TSS. IHC.

Arrowheads indicate cells positive for IHC. Bars = 200 μm.

(D) Density of $CD204^+$ cells

B6: C57BL/6N. MRL: MRL/MpJ. lpr: MRL/MpJ-*Fas*$^{lpr/lpr}$. Each bar represents the mean ± SE (n ≥ 4). Significance with the other age in B6 mice (∗), MRL mice (†), and lpr mice (#) or with B6 mice (B), MRL mice (M), and lpr mice (l) at the same age (Kruskal-Wallis followed by Scheffe's test, $P<0.05$).

Figure 7. Fibrosis of TSS

(A–C) Histology of the TSS at high magnification.

Arrows indicate TL. MT staining. Bars = 200 μm.

(D) Thickness of TL.

(E) Density of collagen fibers.

B6: C57BL/6N. MRL: MRL/MpJ. lpr: MRL/MpJ-*Fas*$^{lpr/lpr}$. Each bar represents the mean ± SE (n ≥ 4). Significance with the other age in B6 mice (∗), MRL mice (†), and lpr mice (#) or with B6 mice (B), MRL mice (M), and lpr mice (l) at the same age (Kruskal–Wallis followed by Scheffe's test, $P<0.05$).

Figure 8. Spatiotemporal alternations of TSS.

In B6 mice, reaction and stability phases were relatively clear and TSS was formed. However, at D14, increase of M1-type macrophages were observed and the appearance of foreign body giant cells (FBGR). In MRL mice, as in B6 mice, a stable TSS finally formed. M1-type macrophages decreased. Stable TSS were formed as in other strains, and M1-type macrophages decreased in D14 as in MRL mice. In addition, earlier fibrosis and increased fibrosis than in other strains were

observed.

Supplement figure 1. Measurement method of TL thickness

(A) Schematic image of method to determine the measurement point. ① to ④ denote four measurement points.

(B) Measurement of TLs using image analysis software.

TABLES AND FIGURES

Table 1. Antibodies used in this study

Antibody	Host	Dilution	Source	Antigen retrieval	Blocking serum
Gr-1	Rat	1:800	R and D system, Minnesota, USA	Pepsin	10% normal goat serum
CD3	Rabbit	1:200	Nichirei, Tokyo, Japan	Tris	10% normal goat serum
B220	Rat	1:1600	Cedarlane, Burlington, Canada	Tris	10% normal goat serum
CD31	Rabbit	1:100	Abcam, Cambridge, UK	Tris	10% normal goat serum
CD68	Rabbit	1:500	Abcam, Cambridge, UK	Tris	10% normal goat serum, 5% nomal donkey serum
CD204	Mouse	1:150	TransGenic, Hyogo, Japan	CB	10% normal goat serum, 5% nomal donkey serum
Rat IgG-biotin	Goat	1:300	BioLegend, San Diego, CA, USA		
Rabbit IgG-biotin	Goat	Undiluted	Undiluted SABPOⓇKit, Nichirei, Tokyo, Japan		
Mouse IgG-biotin	Goat	Undiluted	Undiluted SABPOⓇKit, Nichirei, Tokyo, Japan		
Rabbit IgG-Alexa Fluor 488	Donkey	1:500	Thermo Fisher Scientific, Waltham, MA, USA		
Mouse IgG-Alexa Fluor 546	Donkey	1:500	Thermo Fisher Scientific, Waltham, MA, USA		

Pepsin: 0.1% pepsin, 37 ° C, 5min

Tris: 20mM tris(hydroxymeth)aminomethane-HCl(pH9.0), 110° C, 15min

CB: 10mM citrate buffer(pH6.0), 110° C, 15min

Table 2. Correlation between cellular components and fibrosis indices

		Fibrotic indices	
		Thickness of TL	Density of collagen fiber
Cell components	Total cell number	0.398*	-0.481**
	$CD31^+$cell	0.226	-0.325
	$Gr\text{-}1^+$cell	-0.090	-0.267
	$CD68^+$cell	0.463**	-0.587**
	$CD204^+$cell	0.089	-0.573**

Spearman's rank correlation cofficients. ＊:*P* <0.05, ＊＊: *P* <0.01, n=36 (B6, MRL, lpr)

TL: thin layer

Table 3. Correlation between autoimmune indices and various indices

		Autoimmune indices	
		SPW/ BW	Serum anti-dsDNA antibody
Fibrotic indices	Thickness of TL	0.434	-0.315
	Density of collagen fiber	0.315	0.112
Cell components	Total cell number	-0.091	0.119
	$CD31^+$cell	0.049	-0.503
	$Gr\text{-}1^+$cell	-0.524	-0.049
	$CD68^+$cell	-0.168	-0.580*
	$CD204^+$cell	-0.329	0.063

Spearman's rank correlation cofficients. *:P <0.05, n=12 (lpr)

SPW/BW: ratio of spleen weight to body weight

dsDNA: double stranded DNA

TL: thin layer

Fig 1

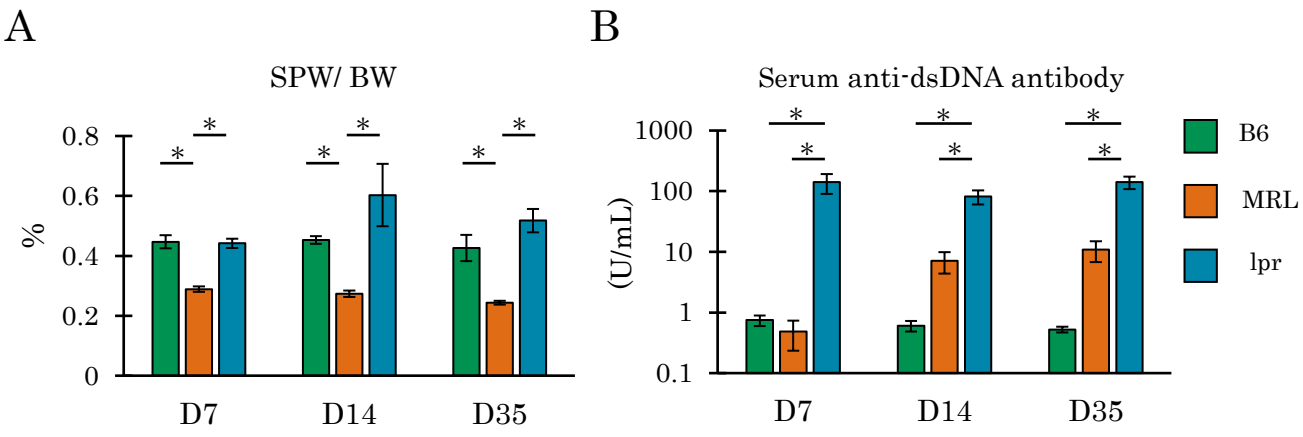
A
SPW/ BW
%
0.8
0.6
0.4
0.2
0
D7
D14
D35
B
Serum anti-dsDNA antibody
(U/mL)
1000
100
10
1
0.1
D7
D14
D35
B6
MRL
lpr

Fig 2

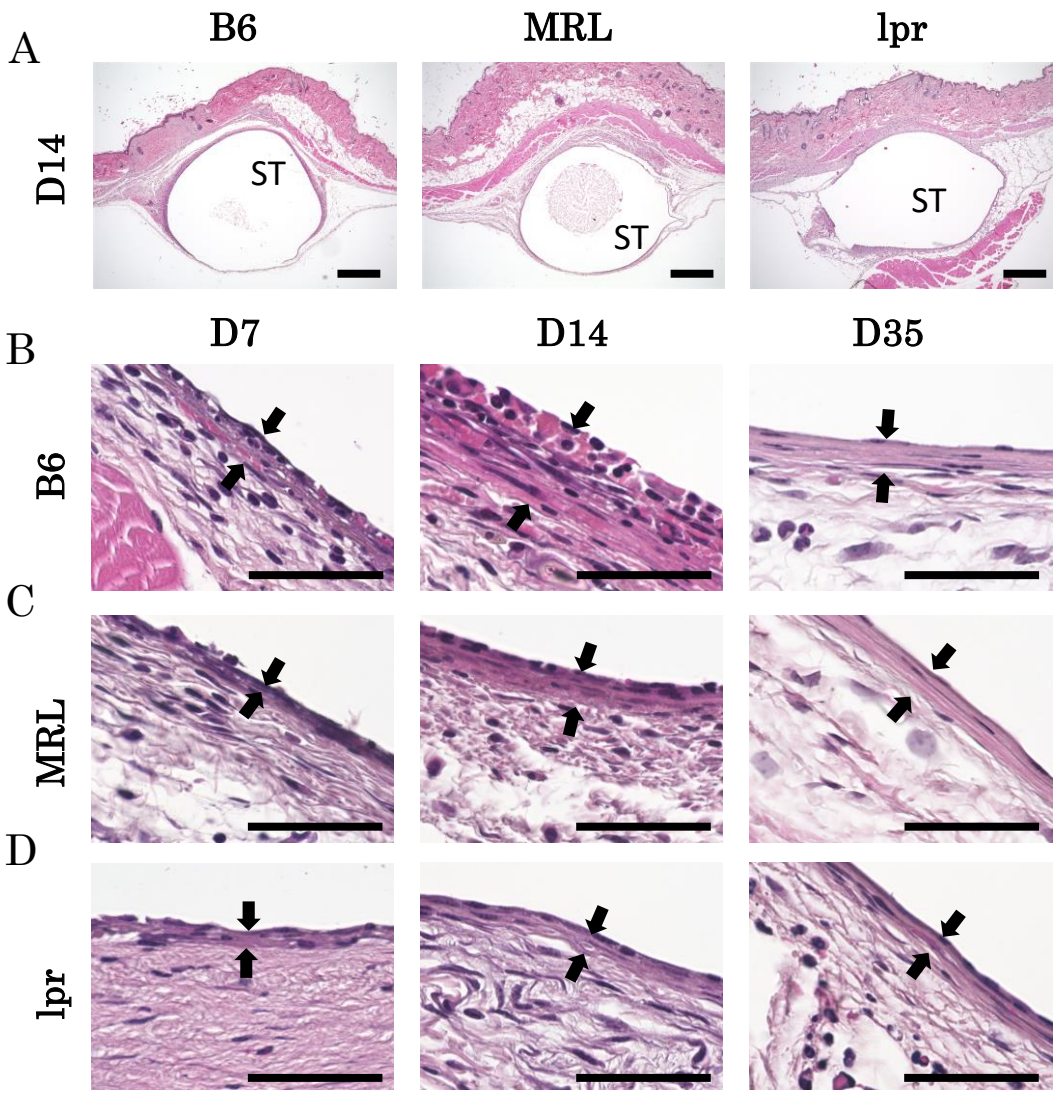
A
B6
MRL
lpr
D14
ST
ST
ST
B
D7
D14
D35
B6
C
MRL
D
lpr

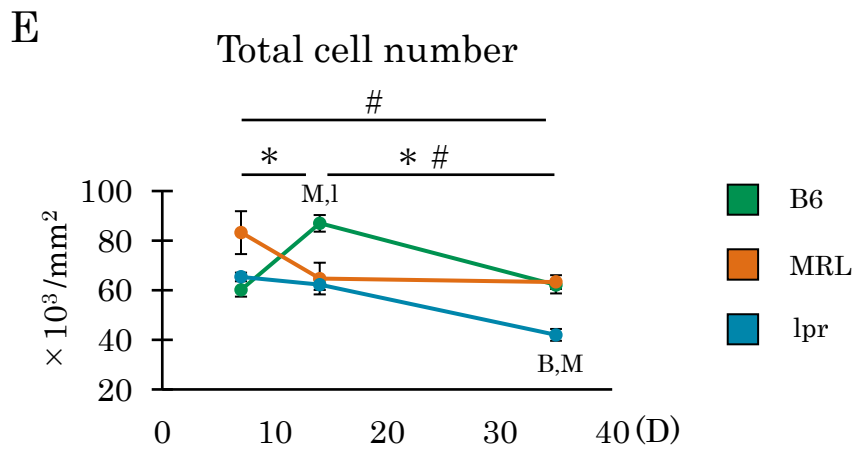
E
Total cell number
#
*
* #
M,l
B,M
100
80
60
40
20
×10³/mm²
0
10
20
30
40 (D)
B6
MRL
lpr

Fig 3

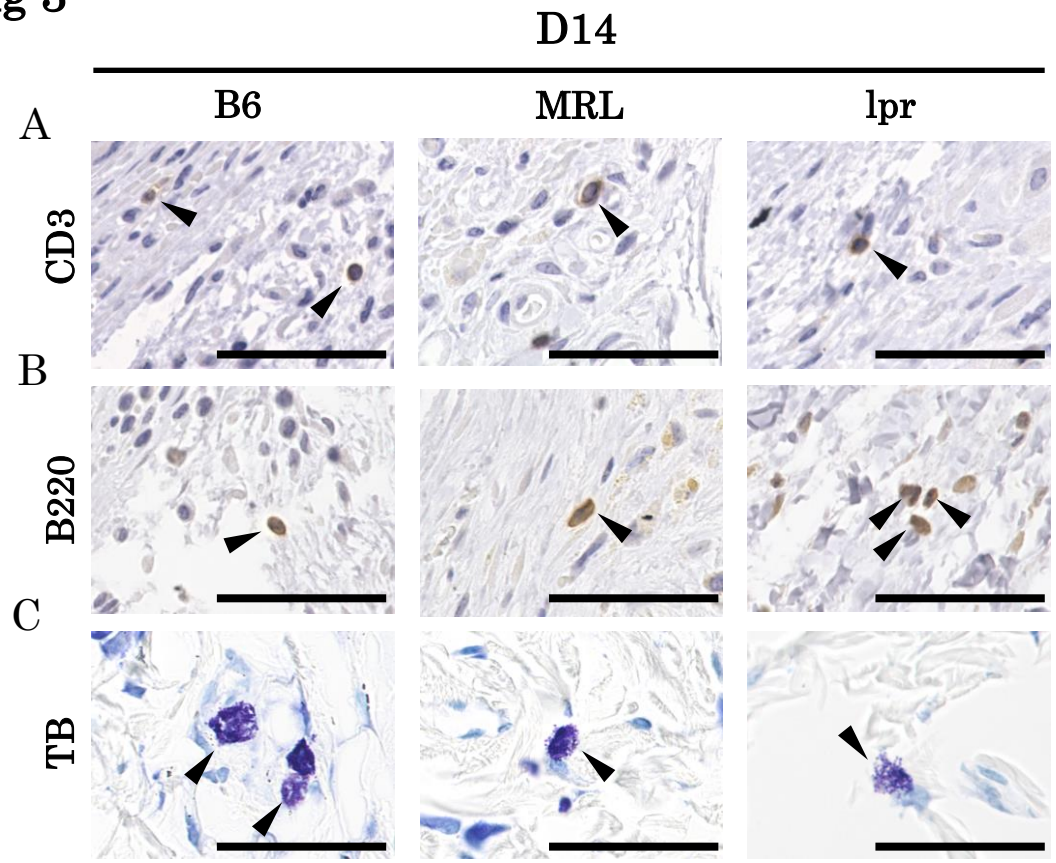

Fig 4

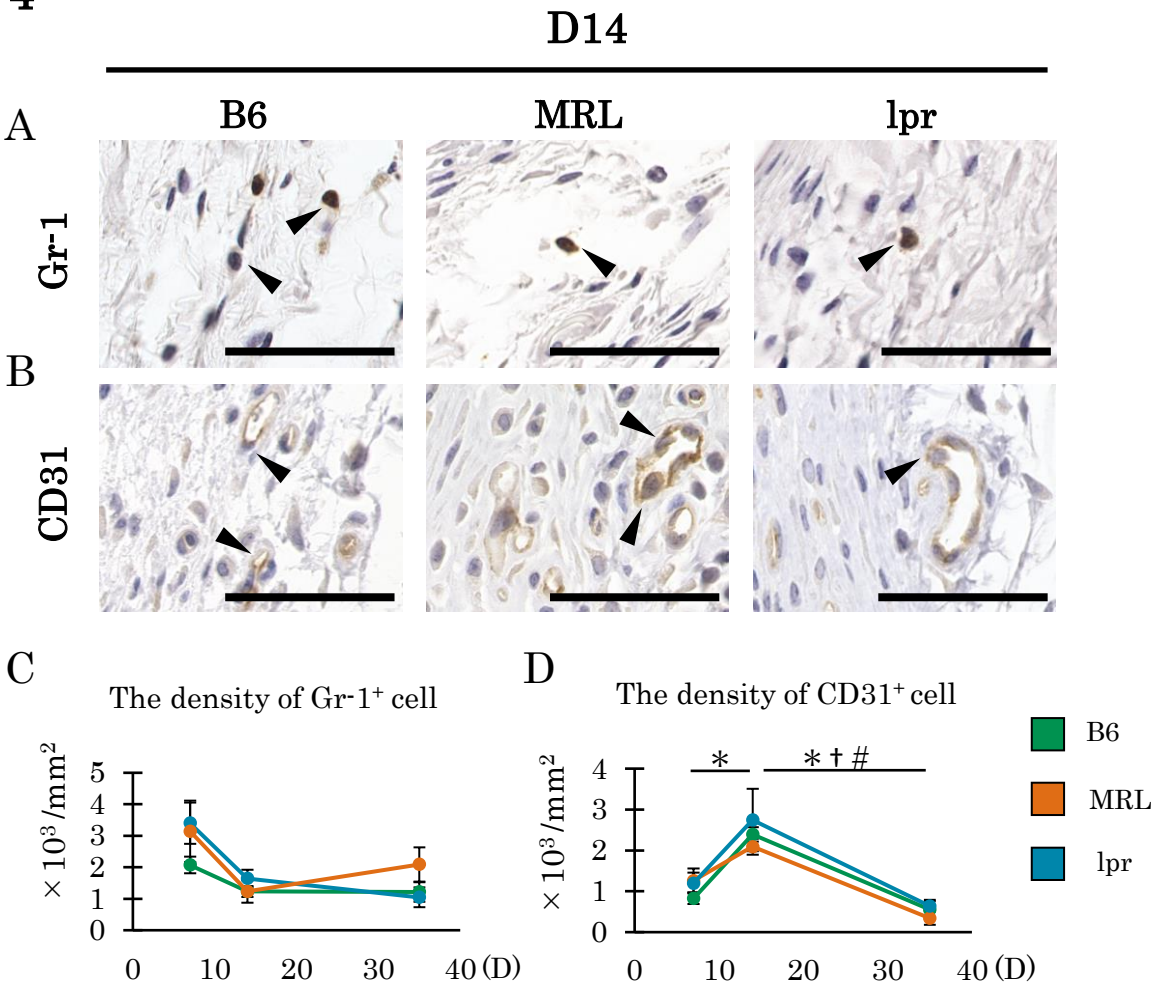
D14
A
B6
MRL
lpr
Gr-1
B
CD31
C
The density of Gr-1+ cell
× 10³ /mm²
5
4
3
2
1
0
0
10
20
30
40 (D)
D
The density of CD31+ cell
× 10³ /mm²
4
3
2
1
0
*
*†#
0
10
20
30
40 (D)
B6
MRL
lpr

Fig 5

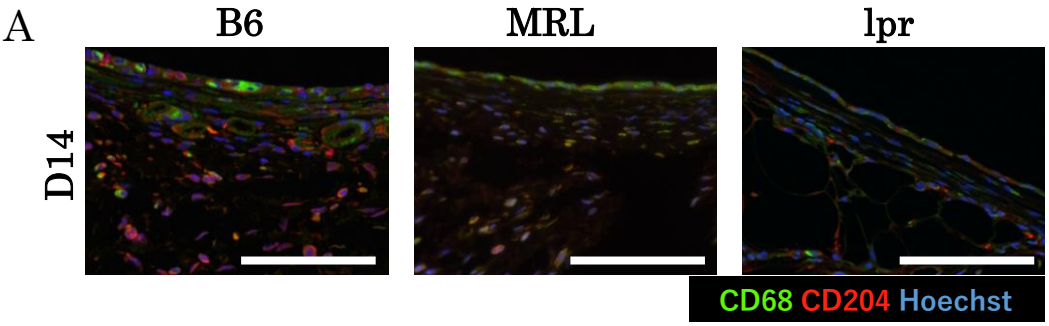
A
B6
MRL
lpr
D14
CD68 CD204 Hoechst

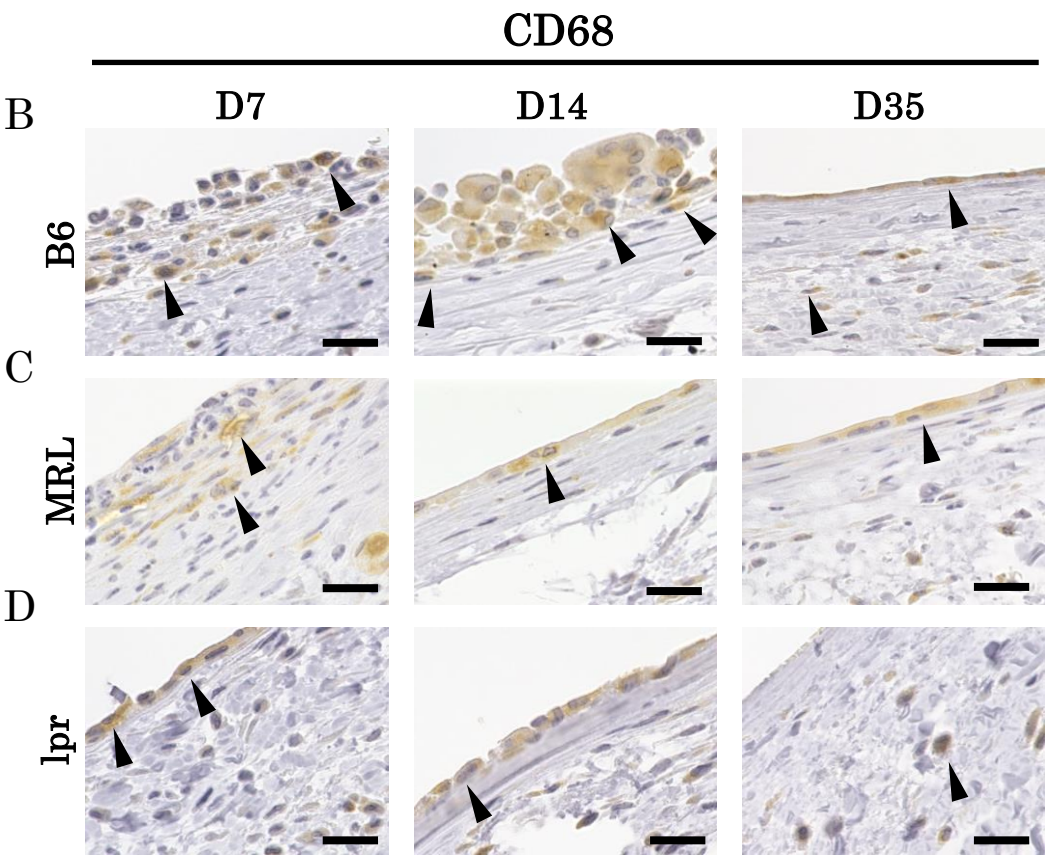
CD68
B
D7
D14
D35
B6
C
MRL
D
lpr

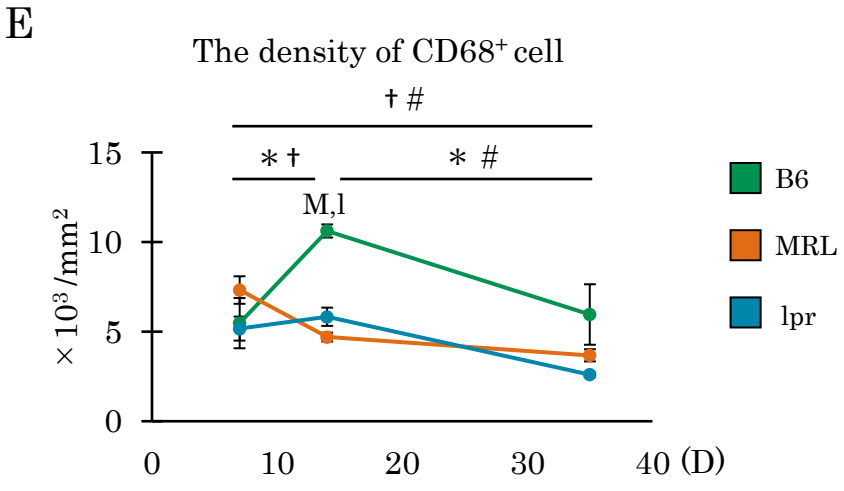
E
The density of CD68+ cell
† #
* †
* #
M,l
15
10
5
0
× 10³/mm²
0
10
20
30
40 (D)
B6
MRL
lpr

Fig 6

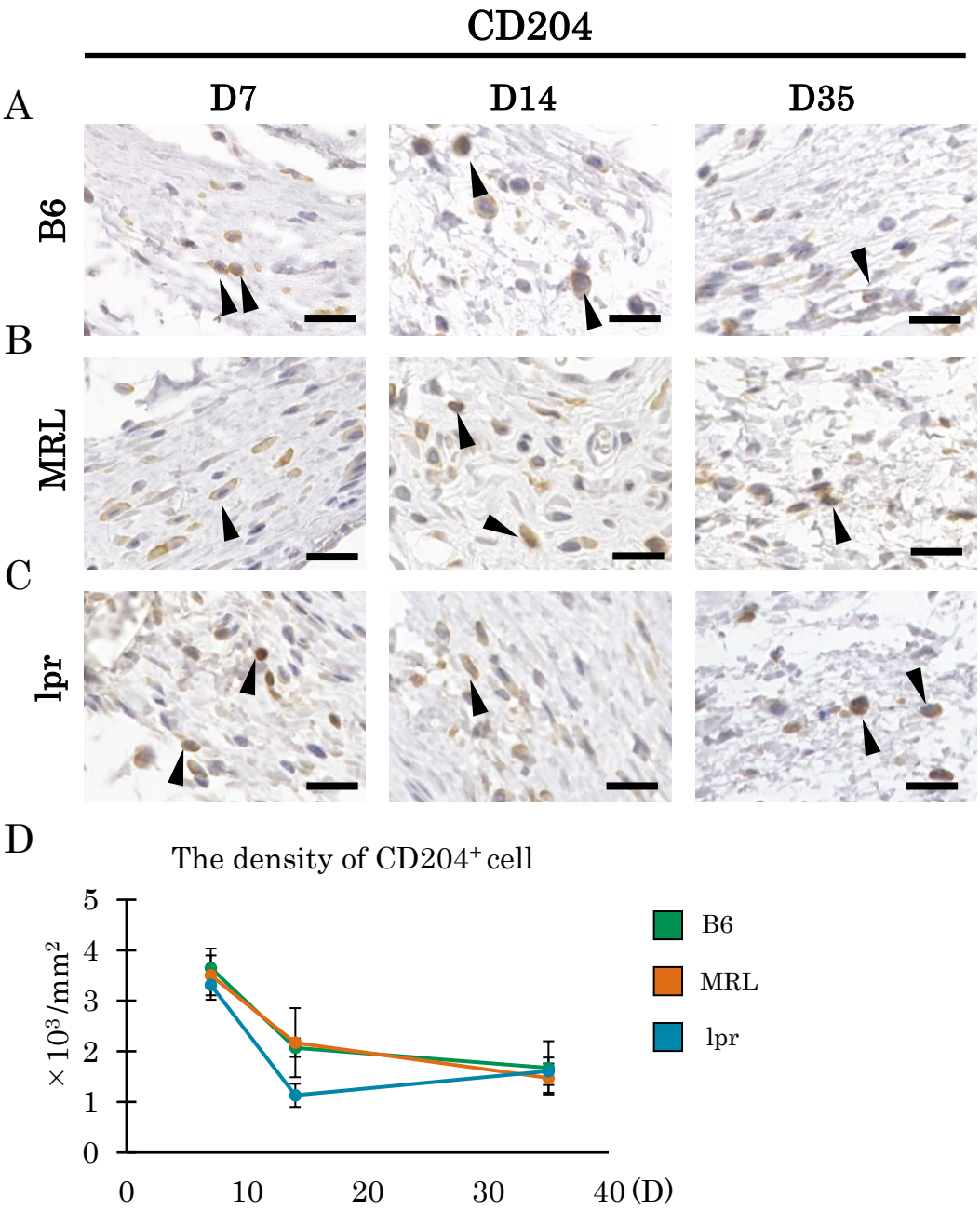
CD204
A
D7
D14
D35
B6
B
MRL
C
lpr
D
The density of CD204+ cell
× 10³/mm²
5
4
3
2
1
0
0
10
20
30
40 (D)
B6
MRL
lpr

Fig 7

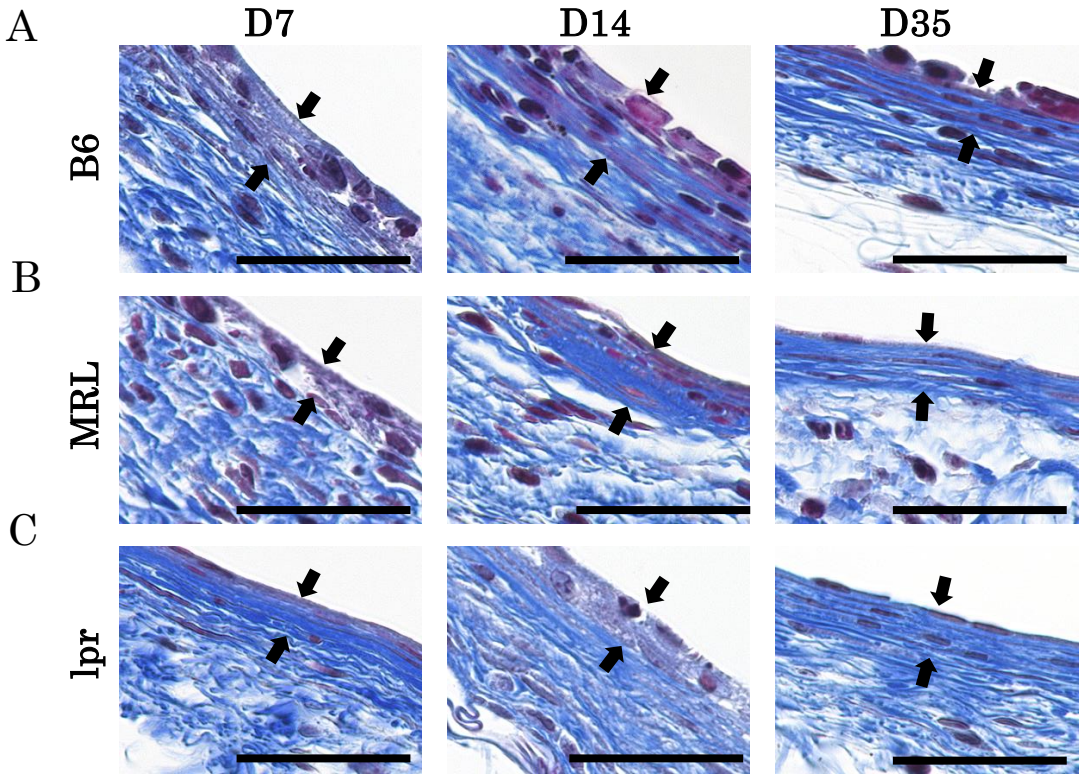
A
D7
D14
D35
B6
B
MRL
C
lpr

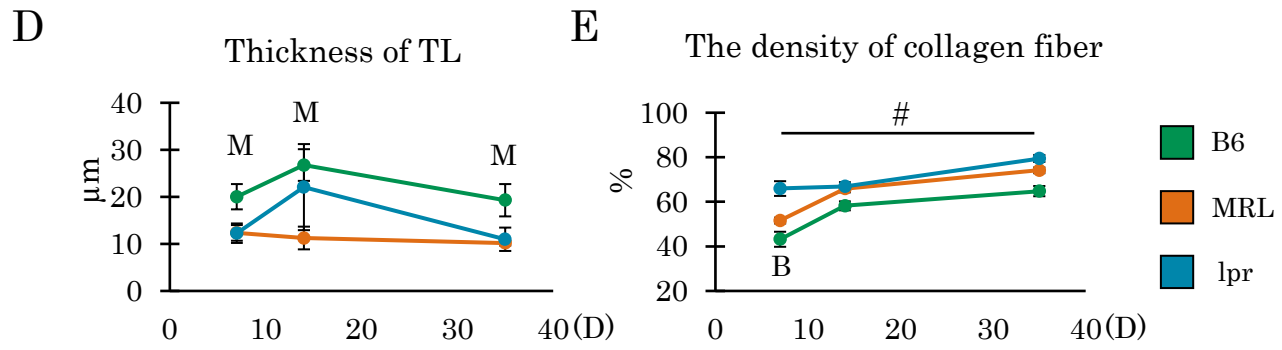
D
Thickness of TL
μm
40
30
20
10
0
M
M
M
0
10
20
30
40(D)
E
The density of collagen fiber
%
100
80
60
40
20
#
B
0
10
20
30
40(D)
B6
MRL
lpr

Fig 8

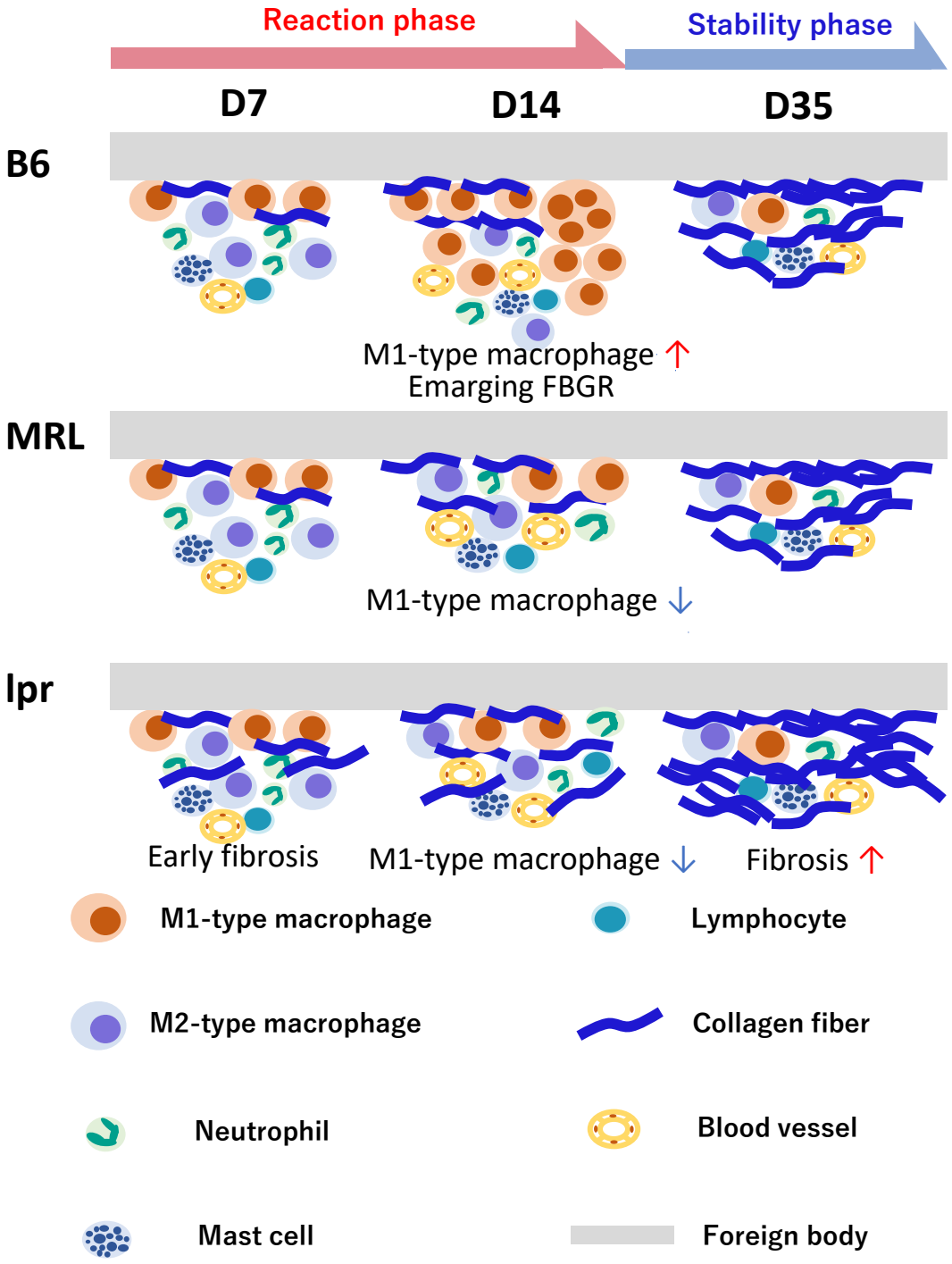
Reaction phase
Stability phase
D7
D14
D35
B6
M1-type macrophage ↑
Emarging FBGR
MRL
M1-type macrophage ↓
lpr
Early fibrosis
M1-type macrophage ↓
Fibrosis ↑
M1-type macrophage
Lymphocyte
M2-type macrophage
Collagen fiber
Neutrophil
Blood vessel
Mast cell
Foreign body

Supplemental figure 1

A

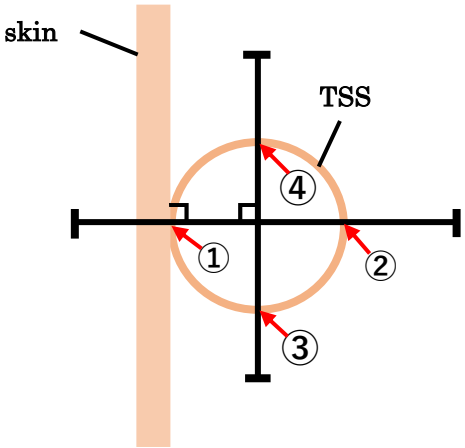

B